Neuro-Oncology

22(1), 58–69, 2020 | doi:10.1093/neuonc/noz151 | Advance Access date 26 August 2019

MEK/MELK inhibition and blood–brain barrier deficiencies in atypical teratoid/rhabdoid tumors

Michaël H. Meel, Miriam Guillén Navarro, Mark C. de Gooijer, Dennis S. Metselaar, Piotr Waranecki, Marjolein Breur, Tonny Lagerweij, Laurine E. Wedekind, Jan Koster, Marianne D. van de Wetering, Netteke Schouten-van Meeteren, Eleonora Aronica, Olaf van Tellingen, Marianna Bugiani, Timothy N. Phoenix, Gertjan J. L. Kaspers, and Esther Hulleman

Departments of Pediatric Oncology/Hematology, Cancer Center Amsterdam, Amsterdam University Medical Centers, Amsterdam, Netherlands (M.H.M., M.G.N., D.S.M., P.W., G.J.L.K., E.H.); Princess Máxima Center for Pediatric Oncology, Utrecht, Netherlands (M.H.M., D.S.M., P.W., M.D.v.W., N.S-v.M., G.J.L.K., E.H.); Division of Pharmacology/Mouse Cancer Clinic, The Netherlands Cancer Institute, Amsterdam, Netherlands (M.C.d.G., O.v.T.); Department of Pathology, Amsterdam University Medical Centers, Amsterdam, Netherlands (M.B., M.Bu.); Department of Neurosurgery, Neuro-oncology Research Group, Cancer Center Amsterdam, Amsterdam University Medical Centers, Amsterdam, Netherlands (T.L., L.E.W.); Department of Oncogenomics, Amsterdam University Medical Centers, Amsterdam, Netherlands (J.K.); Department of Pediatric Oncology, Academic Medical Center, Emma Children's Hospital, Amsterdam, Netherlands (M.D.v.W., N.S-v.M.); Department of (Neuro) Pathology, Amsterdam University Medical Centers, University of Amsterdam, Amsterdam, Netherlands (E.A.); Division of Pharmaceutical Sciences, College of Pharmacy, University of Cincinnati/Research in Patient Services, Cincinnati Children's Hospital Medical Center, Cincinnati, Ohio, USA (T.N.P.)

Corresponding Author: Dr. Esther Hulleman, Heidelberglaan 25 3584CS Utrecht The Netherlands (e.hulleman@prinsesmaximacentrum.nl).

Abstract

Background. Atypical teratoid/rhabdoid tumors (AT/RT) are rare, but highly aggressive. These entities are of embryonal origin occurring in the central nervous system (CNS) of young children. Molecularly these tumors are driven by a single hallmark mutation, resulting in inactivation of *SMARCB1* or *SMARCA4*. Additionally, activation of the MAPK signaling axis and preclinical antitumor efficacy of its inhibition have been described in AT/RT.

Methods. We established and validated a patient-derived neurosphere culture and xenograft model of sonic hedgehog (SHH) subtype AT/RT, at diagnosis and relapse from the same patient. We set out to study the vascular phenotype of these tumors to evaluate the integrity of the blood–brain barrier (BBB) in AT/RT. We also used the model to study combined mitogen-activated protein kinase kinase (MEK) and maternal embryonic leucine zipper kinase (MELK) inhibition as a therapeutic strategy for AT/RT.

Results. We found MELK to be highly overexpressed in both patient samples of AT/RT and our primary cultures and xenografts. We identified a potent antitumor efficacy of the MELK inhibitor OTSSP167, as well as strong synergy with the MEK inhibitor trametinib, against primary AT/RT neurospheres. Additionally, vascular phenotyping of AT/RT patient material and xenografts revealed significant BBB aberrancies in these tumors. Finally, we show in vivo efficacy of the non-BBB penetrable drugs OTSSP167 and trametinib in AT/RT xenografts, demonstrating the therapeutic implications of the observed BBB deficiencies and validating MEK/MELK inhibition as a potential treatment.

Conclusion. Altogether, we developed a combination treatment strategy for AT/RT based on MEK/MELK inhibition and identify therapeutically exploitable BBB deficiencies in these tumors.

Key Points

1. The first primary SHH subtype AT/RT culture and xenograft model has been established.
2. MEK/MELK is identified as a therapeutic strategy for AT/RT.
3. There are functional and therapeutically relevant BBB abnormalities in AT/RT.

Importance of the Study

Atypical teratoid/rhabdoid tumors are currently only curable in a subset of patients by intensive, empiric, chemo- and radiotherapy, resulting in severe long-term side effects. Owing to the lack of knowledge on the disease, only few specific therapeutic targets are known. One such therapeutic target is the mitogen-activated protein kinase pathway, which is aberrantly activated by overexpression of LIN28. We identify MELK as a therapeutic target in these tumors and demonstrate a strong antitumor synergy between the MELK inhibitor OTSSP167 and the MEK inhibitor trametinib. We furthermore demonstrate that the BBB in AT/RT xenografts is disrupted, allowing for the treatment of xenograft-bearing mice with trametinib and OTSSP167, which poorly cross an intact BBB. Our study shows that combined MEK and MELK inhibition is a potential targeted treatment strategy for AT/RT, and demonstrates the possibility to exploit functional BBB deficiencies in AT/RT in a therapeutic manner.

Atypical teratoid/rhabdoid tumors (AT/RT) are highly aggressive pediatric brain tumors that generally occur at a very young age (0–3 y) and carry a dismal prognosis.[1–3] Recent scientific progress demonstrated that intensive multimodal treatment regimens may result in long-term survival, albeit at the cost of severe long-term sequelae.[2,3] On a molecular level, AT/RT arises from a single genetic event, causing a loss of expression of SWItch/sucrose nonfermentable related, matrix associated, actin dependent regulator of chromatin, subfamily B (SMARCB1) or, infrequently, SMARCA4, which are both involved in chromatin remodeling. This loss results in a global (epi)genetic dysregulation and drives malignant transformation in these tumors.[4,5] Recently, genome-wide methylation profiling and RNA sequencing studies have revealed the existence of 3 molecular subtypes of AT/RT: Group 1/sonic hedgehog (SHH), Group 2A/tyrosinase, and Group 2B/MYC.[6,7] These subgroups correlate with differential pathway activation and localization within the CNS, but the prognostic significance remains to be determined. Additionally, AT/RT are characterized by high levels of LIN28, an RNA-binding protein that inhibits the *let7* family of miRNAs, thereby causing the upregulation of multiple oncogenes.[8,9] In particular, LIN28 is responsible for the activation of the mitogen-activated protein kinase (MAPK) and phosphatidylinositol-3 kinase pathways in AT/RT. Inhibition of critical components of these pathways has been shown to be an effective therapeutic strategy in preclinical studies of AT/RT.[9,10] Recently, we described the maternal embryonic leucine zipper kinase (MELK), normally expressed only during embryonic CNS development, as a novel therapeutic target in diffuse intrinsic pontine glioma and demonstrated the efficacy of the MELK inhibitor OTSSP167 in treating preclinical models of this tumor.[11] MELK has previously been identified as a therapeutic target in various types of cancer, where it is involved in a broad variety of cellular processes, ranging from (epi)genetic regulation to cell cycle progression and maintenance of cancer stem cell characteristics.[12–17] In particular, in vivo studies have shown a potent antitumor effect of OTSSP167 on the growth of lung, pancreas, breast, and prostate cancer xenografts.[17] Moreover, local delivery of siomycin A or compound C1, two other MELK inhibitors, as well as MELK knockdown, had a significant antitumor effect on glioblastoma xenografts.[18–20] Two studies have identified MELK as a downstream effector of the MAPK signaling pathway, either via direct phosphorylation of MELK by MAP kinases, or induction of transcription by upregulation of the transcription factor E2F1.[12,14] In the current study, we describe the establishment of an SHH subtype AT/RT neurosphere and xenograft model and explore the vascular phenotype and blood–brain barrier (BBB) integrity of this AT/RT model. We validate our findings using the established CHLA-AT/RT-06 cell line. Additionally, we evaluate MELK as a therapeutic target in AT/RT in combination with MEK inhibition, thereby exploiting the BBB deficiencies observed in these devastating tumors.

Materials and Methods

Cell Lines and Culture Conditions

The VUMC-AT/RT-01 and -01R cultures were established from surgical tissue of an AT/RT patient at the Amsterdam University Medical Center as described previously.[21] Patient material and data were collected in accordance with the Declaration of Helsinki. The CHLA-AT/RT-02 and CHLA-AT/RT-04 cultures, both Group 1/SHH subtype, and the Group 2B/MYC subtype culture CHLA-AT/RT-06[7] were obtained from the American Type Culture Collection. All cell cultures show a loss of *SMARCB1*, as is typically seen in AT/RT. AT/RT cultures were maintained as neurospheres in serum-free medium, as previously described for other pediatric brain tumors.[11,21,22] All cultures were routinely subjected to mycoplasm testing and only used for experiments when confirmed negative. Routine short tandem repeat analysis was performed using the Geneprint 10 system (Promega) to ensure cell line identity. VUMC-AT/RT-01 cells were lentivirally transduced using the pHIV-Luc-ZsGreen (Addgene #39196) plasmid, as previously described.[22]

Drugs and Solutions

OTSSP167 hydrochloride was purchased from Medchem Express; trametinib was obtained from Axon Medchem; PD0325901, SCH772984, and dabrafenib were from Selleckchem. For in vitro experiments, drugs were dissolved in 100% dimethyl sulfoxide (DMSO), and a maximum final concentration of 0.1% DMSO was allowed during experiments. For in vivo experiments, drugs were dissolved in NaCl 0.9% containing a final concentration of 10% DMSO.

Cell Viability Assays

Cell viability assays were performed as previously described.[11] For MELK knockdown experiments, AT/RT neurospheres were lentivirally transduced with previously validated short hairpin (sh)MELK constructs, and growth curves were generated as described.[11] MELK knockdown was confirmed by quantitative PCR (forward primer: GCAGATGTTTGGAGCATGGG, reverse primer: ATCCGTTTCTTTGGGTCCAC).

Western Blot Analysis

Cells were harvested under optimal growth conditions for all western blots, or after 24 h exposure to OTSSP167 and/or trametinib when stated. Western blotting was performed as previously described,[11] using the following primary antibodies: 1:500 rabbit anti-MELK polyclonal antibody(Cell Signaling Technology #2274), 1:1000 rabbit anti-phospho-ERK1/2$^{T202/Y204}$ polyclonal antibody(Cell Signaling Technology #9101), and 1:2000 rabbit anti-ERK1/2 monoclonal antibody (Cell Signaling Technology, clone 137F5, #4695). Additionally, membranes were incubated with 1:5000 anti-actin mouse monoclonal antibody (clone C4, Millipore) or anti–α-tubulin (clone DM1A, Sigma Aldrich, #T6199) as a loading control. Quantification of bands was performed using ImageJ.

Next Generation Sequencing

DNA methylation arrays and copy number profiles were performed and analyzed as previously described, using the Heidelberg classifier.[6] Publicly available gene expression datasets of AT/RT patient samples (n = 18[23] and n = 49[6]), encompassing tumors of all AT/RT subtypes, were uploaded to the R2 platform and used to demonstrate overexpression of MELK. For RNA sequencing experiments, optimally growing VUMC-AT/RT-01 and VUMC-AT/RT-01R neurospheres were treated for 24 hours with 5 nM OTSSP167, 5 nM trametinib, or the combination thereof, after which RNA was extracted and sequencing performed as previously described.[11]

Animals

All animal experiments were approved by local and governmental animal experimental committees and carried out according to national and institutional guidelines. Animals were provided food and water ad libitum for the entire duration of the experiments.

In Vivo Modeling Studies

Female athymic nude mice (BALB/c outbred background, Envigo) were injected intracranially with 500 000 VUMC-ATRT-01 or CHLA-AT/RT-06 cells. The stereotactic coordinates that were used to inject into the cerebellum (VUMC-AT/RT-01) were 1 mm laterally, 2.3 mm caudally, and 2.5 mm ventrally from the lambda. Coordinates for striatal injections (CHLA-AT/RT-06) were 2 mm laterally, –0.5 mm caudally, and 3 mm ventrally from the bregma. Cells were injected in an injection volume of 5 μL at a flow rate of 2.5 μL/minute to minimize the neurological side effects of the procedure, as well as potential backflow of cells. At humane endpoints, when mice developed neurological symptoms, mice were anesthetized by ketamine/xylazine and subsequently euthanized by cardiac puncture and perfusion with 4% paraformaldehyde (PFA) in phosphate buffered saline (PBS). Brains were collected and fixed in 4% PFA afterward for immunohistochemistry and immunofluorescence.

In Vivo Efficacy Studies

Female athymic nude mice (BALB/c outbred background, Envigo) were intracranially injected with 500 000 VUMC-ATRT-01-Fluc cells as described above. Engraftment of xenografts was determined by bioluminescence imaging using the Bruker Xtreme In Vivo imaging system 10 minutes after intraperitoneal injection of 100 mg/kg D-luciferin (GoldBio). Two weeks after injection of tumor cells, xenografts were established and mice were stratified into 4 groups receiving either vehicle, 5 mg/kg/d OTSSP167, 0.75 mg/kg/d trametinib, or the combination of both for 5 consecutive days, followed by a washout period of 5 days and a second course of the same treatment lasting another 5 days. Survival was scored based on humane endpoints, when mice lost >20% body weight or displayed severe neurological symptoms.

Immunohistochemistry

Whole mouse heads were fixed overnight in a solution containing 4% (v/v) PFA and 5% (v/v) glacial acetic acid. Samples were subsequently decalcified using a 6.5% (v/v) formic acid solution for 4 days at 37°C. Decalcified tissues were paraffin embedded and cut into 4 μm coronal sections that were stained with hematoxylin and eosin, and for SMARCB1 (1:100; 612111, BD Biosciences), MELK (1:50; ab129373, Abcam), Ki-67 (1:3000; ab15580, Abcam), glial fibrillary acidic protein (GFAP) (1:500; BT46-5002–04, BioTrend), S100 (1:1000; Z0311, DakoCytomation), human vimentin (1:4000; M0725, DakoCytomation), cytokeratin-5/6 (1:100; M7237, DakoCytomation), breast cancer resistance protein (BCRP) (1:1000; ab24115, Abcam), permeability glycoprotein (P-gP) (1:1000, #13978, Cell Signaling Technologies), claudin 5 (CLDN5) (1:50; 34–1600, Invitrogen), and glucose transporter 1 (GLUT1) (1:100–2000; 07-1401, Millipore). Tumor and normal brain tissue from the patient were collected in 4% (v/v) PFA and processed and stained for GLUT1 and CLDN5 as previously described.[24]

Immunofluorescence

Upon development of neurological symptoms, tumor-bearing mice were anesthetized and perfused with 4% (v/v) PFA, after which brains were collected. Brains were post-fixed in 4% PFA overnight and cryoprotected in 30% sucrose for 24 hours before embedding in tissue freezing media (Electron Microscopy Sciences). Fifty-micrometer-thick floating sections were prepared on a cryostat (Leica).

Sections were blocked in PBS containing 0.5% Triton X-100 with 10% normal donkey serum, and incubated with appropriate primary antibodies: cluster of differentiation 31 (CD31) (1:100; BD Pharmigen #550274), GLUT1 (1:500; EMD Millipore #07-1401), CLDN5–Alexa 488 conjugate (1:250; Life Technologies #352588), and Hoechst (1:1000; Life Technologies #33342). All secondary antibodies (Jackson ImmunoResearch) were used at 1:500. Sections were mounted with ProLong Gold antifade reagent (Life Technologies) and imaged on a Nikon A1 confocal microscope. Images were processed in ImageJ (National Institutes of Health). Vascular density was quantified by measuring the percent area of CD31 staining per field. Vessel diameter was quantified by measuring individual vessels with the linear measuring tool in ImageJ.

Statistical Analysis

Relative cell viabilities and gene expression levels were compared using the independent two-sided *t*-test. Growth curves of shRNA-transduced neurospheres were compared by multilevel regression analysis as previously described.[11] Drug synergy was calculated using the Highest Single Agent formula in SynergyFinder (http://synergyfinder.fimm.fi), which was the most appropriate formula for the reported dose-response curves.[25] Vessel densities were compared by Mann–Whitney *U*-test, whereas vessel diameters were compared by Dunnett's multiple comparisons test. For survival studies, Kaplan–Meier curves were generated and significance of survival differences was determined using the log-rank (Mantel–Cox) test. Statistical analyses were performed with Microsoft Excel, GraphPad Prism (v6), and SPSS (v22), and a *P*-value of <0.05 (two-sided where relevant) was considered statistically significant.

Results

Establishment of a Primary

AT/RT culture and xenograft model.—To study the potential of MELK and MEK inhibition in AT/RT, we established a paired diagnosis-relapse neurosphere culture and patient-derived xenograft (PDX) model of the disease. The VUMC-AT/RT-01 model was derived from tissue of a 3-year-old boy undergoing surgery for a large AT/RT, encompassing the parietal and occipital lobes of the left hemisphere (Fig. 1A, left panel). After surgery, the patient underwent chemotherapy according to the EURHAB2010 protocol, containing doxorubicin, ifosfamide, carboplatin, etoposide, vincristine, cyclophosphamide, actinomycin-D, and intraventricular/intrathecal methotrexate. After 5 months the patient experienced a relapse and was operated again. The second AT/RT neurosphere model, VUMC-AT/RT-01R, was generated from surgical tissue at this timepoint. DNA methylation pattern analysis classified both the VUMC-AT/RT-01 patient tumor tissue and VUMC-AT/RT-01 neurospheres as SHH subtype AT/RT with calibrated methylation class scores of 0.99 and 0.93, respectively. Additionally, genome-wide copy number analysis demonstrated identical copy number variations between the original tumor tissue and VUMC-AT/RT-01/-01R neurospheres, validating these cell cultures and related xenograft as a representative model of SHH subtype AT/RT (Supplementary Fig. 1). To generate the VUMC-AT/RT-01 xenograft (PDX) model, tumor cells were injected into the cerebellum of athymic nude mice after several (5–6) passages of the tumor neurospheres in vitro. After 6–8 weeks, mice developed coordination problems, limb weakness and ataxia and started losing weight. At that moment an MRI was performed and mice were sacrificed by perfusion with 4% PFA, after which brains were collected for further study. The MRI scan of the mice revealed a large, T2 hyperintense, sharply demarcated lesion in the hindbrain, resembling the tumor observed in the patient (Fig. 1A). Immunohistochemical analysis of the brains of tumor-bearing mice revealed the typical loss of SMARCB1 in the nuclei of tumor cells (Fig. 1B), as also observed in the original tumor material. Ki-67 staining revealed high numbers of proliferating tumor cells. Furthermore, patches of cells stained positive for the differentiation markers GFAP, S100, vimentin, and keratin 5/6, demonstrating multilineage differentiation of part of the tumor cells, as expected in a tumor of embryonal origin (Fig. 1C). VUMC-AT/RT-01R neurospheres were not capable of forming xenografts in immunodeficient mice. In short, we created and validated a primary culture and PDX model of SHH subtype AT/RT that adequately recapitulates the geno- and phenotype of the patient's tumor.

Combined Inhibition of MEK and MELK Is Synergistically Toxic to AT/RT Cells

Analysis of publicly available gene expression datasets of tumor samples from AT/RT patients revealed a strong overexpression of MELK compared with normal brain and cerebellar tissue (Fig. 2A). Baseline MELK expression was determined by western blotting in Group 1/SHH subtype VUMC-AT/RT-01, -01R and CHLA-AT/RT-02 and -04 cells, and in Group 2B/MYC subgroup CHLA-AT/RT-06 cells (Fig. 2B). MELK expression in VUMC-AT/RT-01 xenografts was confirmed by immunohistochemistry to validate the model for future in vivo studies involving MELK inhibition (Fig. 2C). VUMC-AT/RT-01, CHLA-AT/RT-02 (Group 1/SHH), and CHLA-AT/RT-06 (Group 2B/MYC) cells were subjected to shRNA-mediated MELK knockdown, validated by quantitative PCR, resulting in a significant delay in growth of VUMC-AT/RT-01 spheres and induction of cell death in CHLA-AT/RT-02 and -06 spheres (Fig. 2D). This dependency of AT/RT cells on the kinase creates a potential therapeutic window, as MELK expression does not occur in normal postnatal CNS tissues, and we have previously shown that primary astrocytes are resistant to MELK inhibition.[11] Protein interaction analysis of MELK using an algorithm of the Search Tool for the Retrieval of Interacting Genes/Proteins (STRING) shows a direct relationship between MELK and central components of the MAPK pathway, as has been published previously in other cancer types (Fig. 2E).[12,14] Based on the overexpression of MELK, the antitumor effects of MELK knockdown, and the reported activation of the MAPK signaling pathway in AT/RT, we then determined the antitumor effect of pharmacological MEK and MELK inhibition in vitro using the VUMC-AT/RT-01 and -01R and CHLA-AT/RT-02, -04, and -06 neurosphere cultures.[7,9] Treatment of these 5 AT/RT cultures with the small-molecule MELK inhibitor OTSSP167—which both inhibits

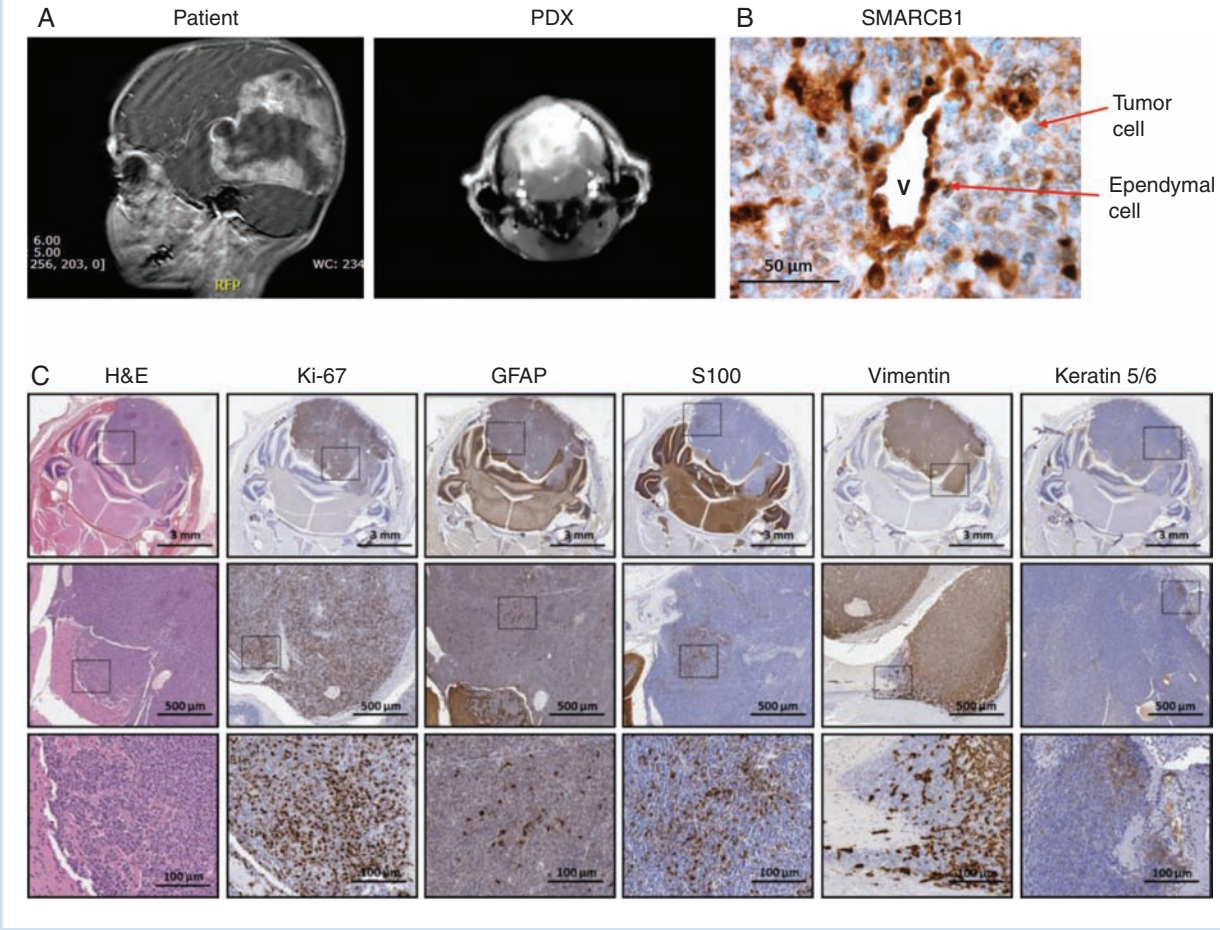

Fig. 1 Establishment of a patient-derived neurosphere and xenograft model of AT/RT (A) T2-weighted MRI of the brain of a 3-year-old AT/RT patient (sagittal view, left panel) and a mouse carrying a VUMC-AT/RT-01 xenograft, derived from tumor cells of this patient (coronal view, right panel). (B) Immunohistochemistry images of the brain of a mouse carrying a VUMC-AT/RT-01 xenograft, showing the typical loss of SMARCB1 expression, in the nuclei of tumor cells. Ependymal cells, with positive nuclear staining of SMARCB1, are shown as a control. (C) Immunohistochemistry images of the brain of a mouse carrying a VUMC-AT/RT-01 xenograft, showing a high proportion of proliferating cells (Ki-67) and patches of multilineage differentiation of tumor cells (GFAP, S100, vimentin, keratin 5/6), as seen in embryonal tumors.

MELK kinase activity and leads to degradation of MELK—and the specific MEK inhibitor trametinib for 96 hours resulted in a strong antiproliferative effect of both inhibitors at low nanomolar concentrations (Supplementary Fig. 2). Whereas the response to OTSSP167 was similar among AT/RT cultures, VUMC-AT/RT-01R spheres were more sensitive to trametinib than the other cultures. Combined treatment of AT/RT cells by OTSSP167 and trametinib resulted in a strong synergistic antiproliferative effect across a range of concentrations (Fig. 3A). Again, the VUMC-AT/RT-01R cells were the most sensitive to combined MEK and MELK inhibition. Similar synergistic antitumor effects were seen in combined treatment of these AT/RT cultures with OTSSP167 and the MEK inhibitor PD0325901 or the extracellular signal-regulated kinase 1 and 2 (ERK1/2) inhibitor SCH772984, whereas the combination with the Raf inhibitor dabrafenib was largely antagonistic (Supplementary Figures 3–5), indicating that inhibition of the MAPK pathway downstream of MEK is essential for the antitumor effect. Taken together, we have identified a dependency of AT/RT cells on MELK and show a synergistic in vitro antitumor effect of combined inhibition of MELK and MEK or ERK1/2 in these cells, which was most prominent in VUMC-AT/RT-01R cells and similar among Group 1/SHH and Group 2B/MYC subgroup cultures.

Reciprocal Effects of MEK and MELK Inhibition in AT/RT Cells

To elucidate the mechanism by which MEK and MELK inhibition exert their synergistic antitumor effect, we exposed VUMC-AT/RT01, -01R, CHLA-AT/RT-02, and CHLA-AT/RT-06 cells for 24 hours to 10 nM OTSSP167, trametinib, or the combination thereof. Analysis of protein levels by western blot (Fig. 3B) revealed the expected decrease in MELK expression in AT/RT cells treated with OTSSP167 and a reduction of phosphorylated (p-)ERK1/2$^{T202/Y204}$ in those treated with trametinib, with the singular exception of a slight increase in MELK levels in CHLA-AT/RT-06 cells treated with OTSSP167 and/or trametinib, indicating that kinase inhibition rather than protein degradation is responsible for the

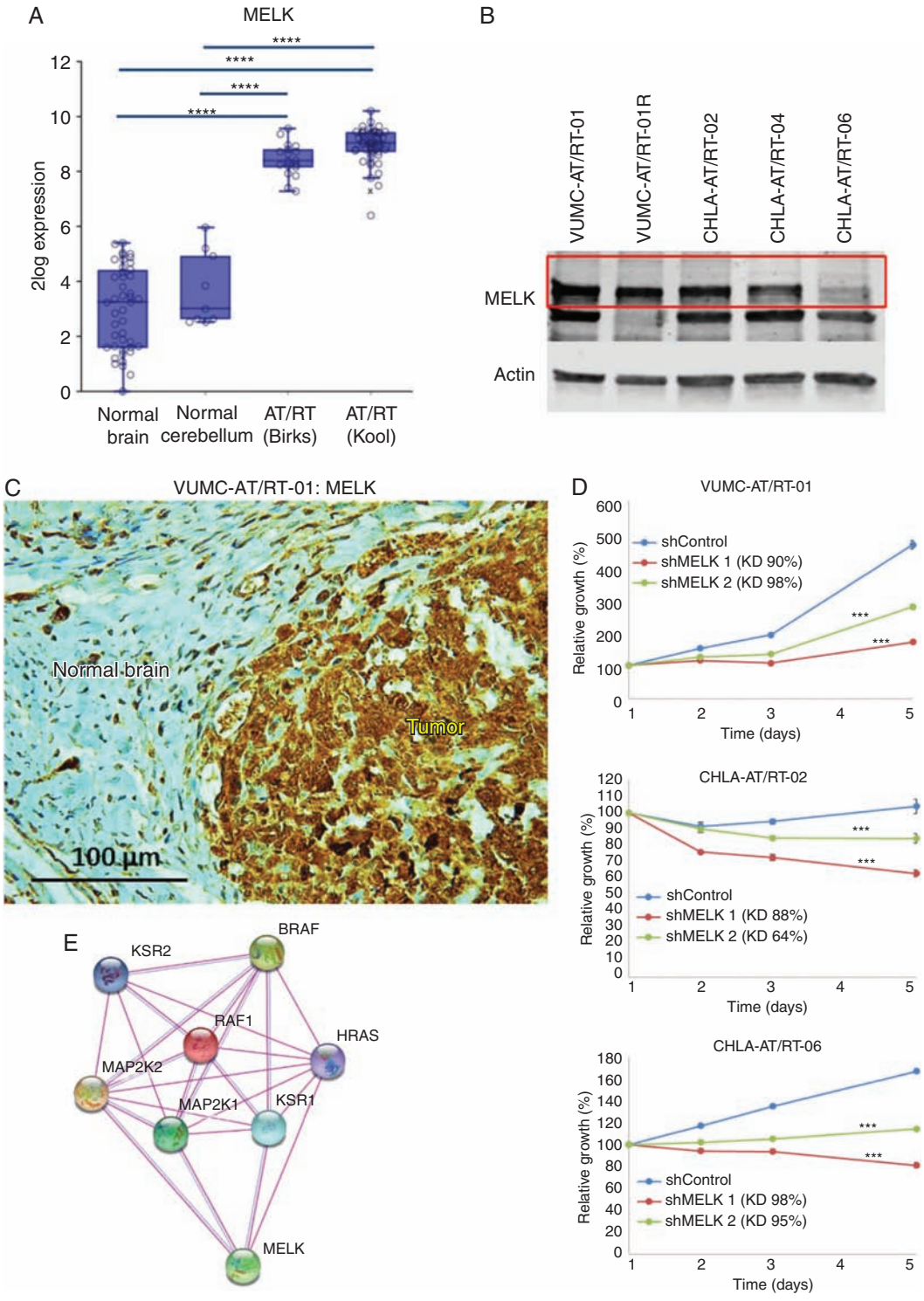

Fig. 2 MELK is overexpressed in AT/RT. (A) mRNA expression levels of MELK in normal brain, cerebellum, and biopsy samples of AT/RT patients (GSE 13564, 3526, 28026, and 70678). Image was generated using R2 (http://r2.amc.nl). ****$P < 0.0001$. (B) Western blot showing baseline MELK expression in VUMC-AT/RT-01, VUMC-AT/RT-01R, CHLA-AT/RT-02, CHLA-AT/RT-04, and CHLA-AT/RT-06 neurospheres. Actin was used as a loading control. Red box outlines full length MELK protein, the lower band likely represents a smaller MELK isoform. (C) Immunohistochemistry images of the brain of a mouse carrying a VUMC-AT/RT-01 xenograft, showing MELK expression in tumor cells. (D) Growth curves of VUMC-AT/RT-01, CHLA-AT/RT-02, and -06 cells after shRNA-mediated knockdown of MELK. Knockdown efficiencies are shown in the graphs. Results are shown as average ± SEM ($n = 6$). ***$P < 0.001$ (multilevel regression analysis). (E) STRING protein interaction analysis (http://string-db.org) of MELK showing known interactions between MELK and MAPK pathway components. Purple connecting lines indicate direct experimental data; blue lines, occurrence in curated databases.

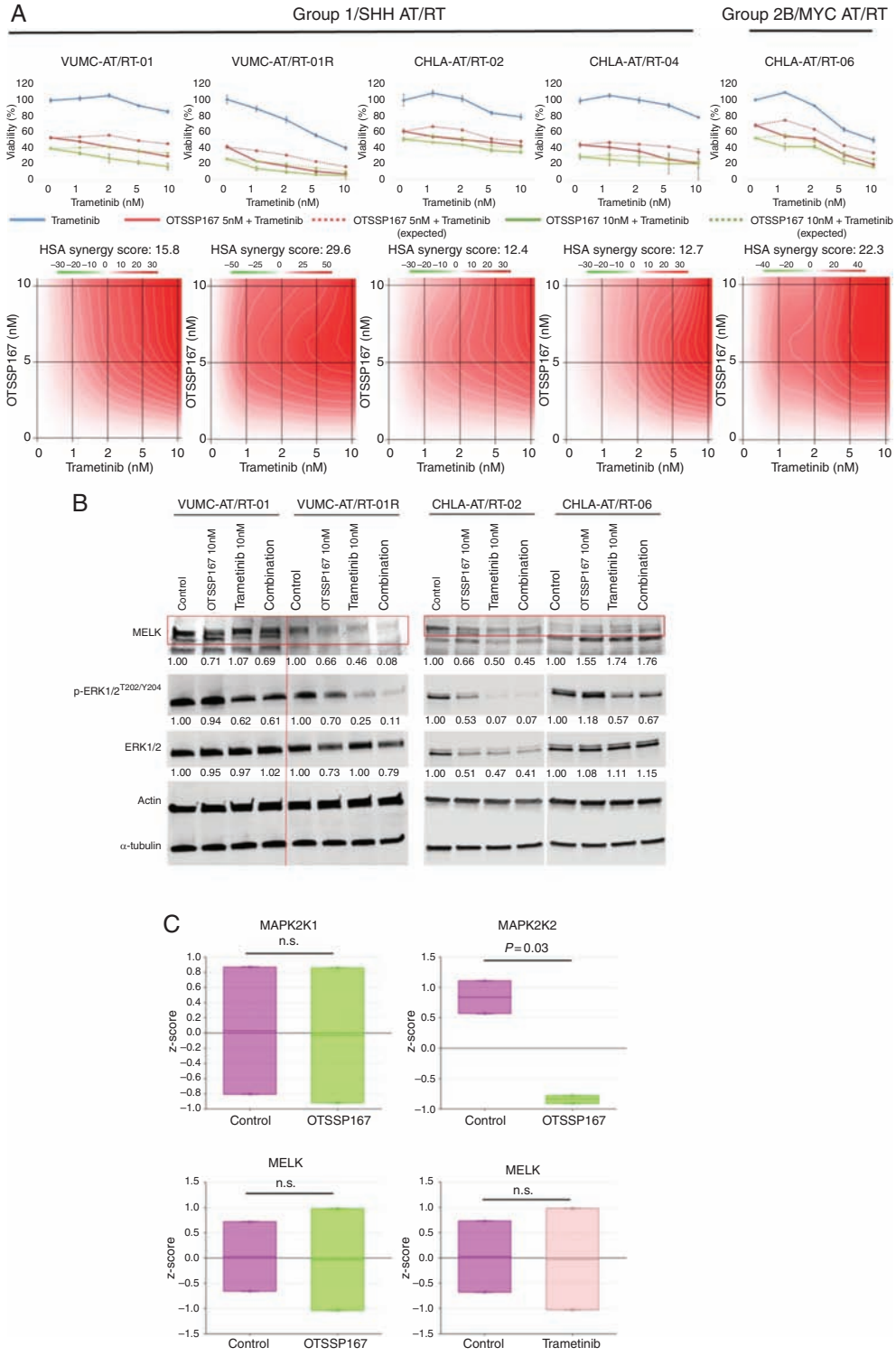

Fig. 3 In vitro efficacy of combined inhibition of MEK and MELK in AT/RT. (A) Upper panels: dose-response curves of VUMC-AT/RT-01, VUMC-AT/RT-01R, CHLA-AT/RT-02, CHLA-AT/RT-04, and CHLA-AT/RT-06 cells exposed for 96 hours to trametinib and 0, 5, or 10 nM OTSSP167. Results are shown as average relative cell viability ± SEM ($n = 5$). Dotted lines represent expected survival of combination treatment assuming additivity. Lower panels: landscape plots of synergy between OTSSP167 and trametinib at different concentrations, belonging to the graphs of the upper panels. Synergy was calculated using the Highest Single Agent (HSA) formula of SynergyFinder (http://synergyfinder.fimm.fi).[25] (B) Western blot showing protein levels of MELK, ERK1/2, and p-ERK1/2$^{T202/Y204}$ in VUMC-AT/RT-01, VUMC-AT/RT-01R, CHLA-AT/RT-02, and CHLA-AT/RT-06 cells treated for 24 hours with 10 nM OTSSP167, 10 nM trametinib, or the combination thereof. Actin and α-tubulin were used as loading controls and to correct quantification, for MELK and (p-)ERK1/2, respectively. (C) RNA sequencing analysis of expression levels of MAP2K1, MAP2K2, and MELK in VUMC-AT/RT-01 and VUMC-AT/RT-01R cells treated for 24 hours with 5 nM OTSSP167 or 5 nM trametinib.

effect of OTSSP167 on these cells. Additionally, treatment of VUMC-AT/RT-01R and CHLA-AT/RT-02 cells with OTSSP167 decreased levels of both ERK1/2 and p-ERK1/2$^{T202/Y204}$. Conversely, treatment of these cells with trametinib resulted in a decrease in MELK expression. RNA sequencing of VUMC-AT/RT-01 and -01R cells treated for 24 hours with 5 nM OTSSP167 or 5 nM trametinib revealed decreased expression of mitogen-activated protein kinase kinase 2 (MAP2K2) (ERK2), but not *mitogen-activated protein kinase kinase 1* (MAP2K1) (ERK1), in AT/RT cells treated with OTSSP167 (Fig. 3C). Expression levels of MELK mRNA were not influenced by either treatment. These results point to a reciprocal interaction between MEK and MELK in AT/RT cells, occurring at both the transcriptional and posttranslational level.

Blood–Brain Barrier Phenotype of AT/RT Xenografts

Based on the promising in vitro antitumor efficacy of OTSSP167 and trametinib, we set out to determine the translational potential of this drug combination for the treatment of AT/RT. As studies have previously shown a very limited BBB penetration of both OTSSP167 and trametinib,[11,26,27] we first determined the BBB integrity of our AT/RT xenograft model. Confocal microscopy of brains of VUMC-AT/RT-01 bearing mice, stained for the endothelial cell marker CD31, revealed a significant decrease in vessel density, as well as an increase in vessel diameter, of intratumoral blood vessels in the tumor (Fig. 4A, D, E), in comparison with surrounding normal brain tissue. Moreover, whereas endothelial cells of intratumoral blood vessels maintained expression of the BBB marker CLDN5, expression of GLUT1 (solute carrier family 2 member 1) was lost on the majority of these cells. Furthermore, staining of CLDN5 revealed that, although expression of this protein is maintained, intratumoral blood vessel endothelial cells display a disorganization of their tight junctions (Fig. 4B, C). These aberrancies in vessel structure and endothelial cell phenotype correspond to a loss of BBB integrity of intratumoral blood vessels in our AT/RT model, in a similar fashion as previously shown for WNT subgroup medulloblastomas.[28] Immunohistochemical analysis of GLUT1 and CLDN5 expression in Group 2B/MYC subtype CHLA-AT/RT-06 xenografts revealed that both

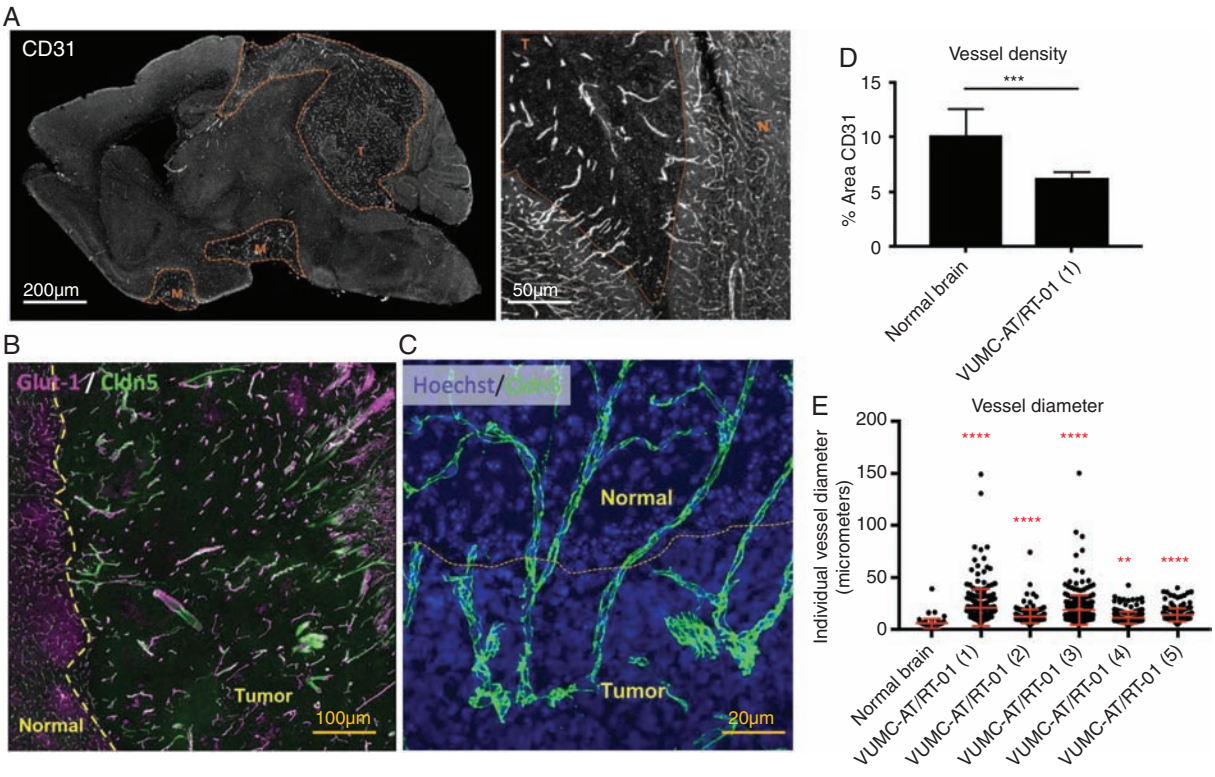

Fig. 4 Abnormal intratumoral blood vessels in AT/RT xenografts. (A) Confocal microscopy images of a sagittal section of the brain of a mouse carrying a VUMC-AT/RT-01 xenograft, stained for the endothelial cell marker CD31, showing reduced density but increased diameter of intratumoral blood vessels. (B) Confocal microscopy image of the brain of a mouse carrying a VUMC-AT/RT-01 xenograft, stained for the blood–brain barrier endothelial cell markers GLUT1 and CLDN5, showing reduced GLUT1 expression in intratumoral blood vessels. (C) Confocal microscopy image of the brain of a mouse carrying a VUMC-AT/RT-01 xenograft, stained for the tight junction protein CLDN5, showing disorganization of tight junctions between endothelial cells of intratumoral blood vessels. (D) Quantification of vessel density, as determined by area of tissue staining positive for CD31, in VUMC-AT/RT-01 xenografts compared with normal brain. ***$P < 0.001$ (Mann–Whitney *U*-test). (E) Quantification of vessel diameter of intratumoral blood vessels in VUMC-AT/RT-01 xenografts compared with blood vessels in normal brain tissue. **$P < 0.01$, ****$P < 0.0001$ (Dunnett's multiple comparisons test).

markers were lost in the majority of intratumoral blood vessels, implying that BBB disruption is not limited to SHH subgroup AT/RT(Supplementary Fig. 6). We then performed immunohistochemical stainings for GLUT1 and CLDN5 on tumor tissue and matching normal brain tissue from the patient from whom the VUMC-AT/RT-01 xenografts were derived (Fig. 5). This revealed a similar loss of GLUT1, but not CLDN5 on endothelial cells of preexisting intratumoral blood vessels. Additionally, in contrast to the xenograft model, areas of microvascular proliferation demonstrated a loss of CLDN5 as well as GLUT1, implying an even stronger loss of BBB integrity. Together, these results point to a defective BBB in AT/RT and validate the VUMC-AT/RT-01 xenografts as a suitable model for the study of the BBB in these tumors.

Efficacy of Combined MEK/MELK Inhibition in AT/RT Xenografts

Given the apparent lack of BBB integrity in our xenograft model of AT/RT, we investigated the therapeutic relevance of the observed intratumoral vascular abnormalities in the context of our proposed combination of MEK and MELK inhibition. For this purpose, we injected VUMC-AT/RT-01-Fluc cells into the cerebellum of athymic nude mice. After 2 weeks, upon demonstration of engraftment by bioluminescence imaging, treatment was started with 5 mg/kg/d OTSSP167 and/or 0.75 mg/kg/d trametinib i.p. for 5 consecutive days, followed by a recovery period of 5 days and a second identical course of treatment. Whereas mice receiving only OTSSP167 or trametinib showed a nonsignificant trend toward improved survival, only mice receiving both compounds had a significantly improved median survival (30 vs 23 days, log-rank test: $P < 0.01$; Fig. 6). Albeit modest, this increase in survival confirms the synergistic antitumor effect of OTSSP167 and trametinib in our AT/RT xenograft model. Moreover, this result demonstrates the relevance of the observed intratumoral vascular abnormalities, as a significant antitumor effect is observed of 2 drugs that do not cross an intact BBB in relevant concentrations. As the BBB penetration of OTSSP167 is mainly limited by the multidrug transporters BCRP and P-gP (multidrug resistance protein 1), we evaluated their expression on endothelial cells in VUMC-AT/RT-01 xenografts and the original tumor tissue. Immunohistochemical staining of these tumors, as well as CHLA-AT/RT-06 xenografts, revealed that P-gP and BCRP expression were partially maintained in intratumoral blood vessels of the PDX tumors. In contrast, BCRP was not expressed in blood vessels of the original tumor, and P-gP was only present in part of the capillaries (Supplementary Figures 7 and 8). As such, the efficacy of OTSSP167 and trametinib seen in the AT/RT PDX model is likely dampened by the presence of multidrug transporters that are not expressed in the patient tumor material.

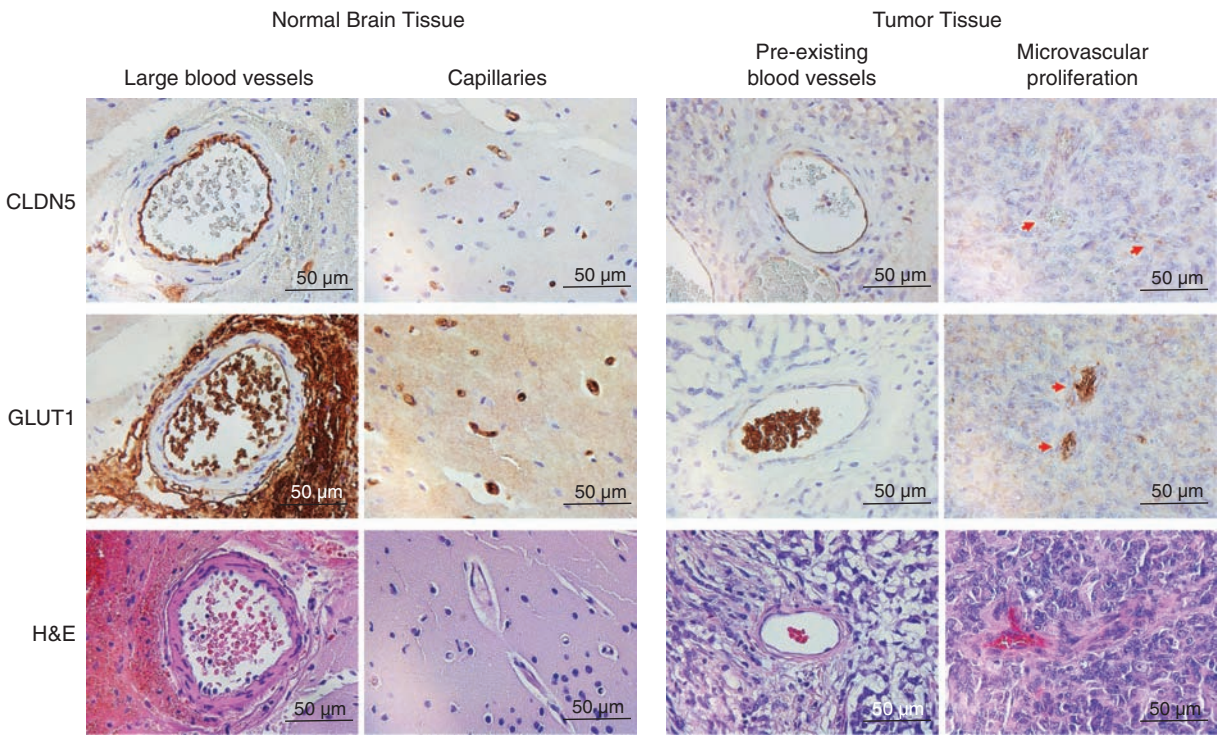

Fig. 5 Abnormal intratumoral blood vessels in AT/RT tumor tissue. Immunohistochemical staining of GLUT1 and CLDN5 in tumor and normal brain tissue from the VUMC-AT/RT-01 patient showing a loss of GLUT1 in endothelial cells of preexisting blood vessels in the tumor, and a loss of both GLUT1 and CLDN5 in endothelial cells in areas of microvascular proliferation.

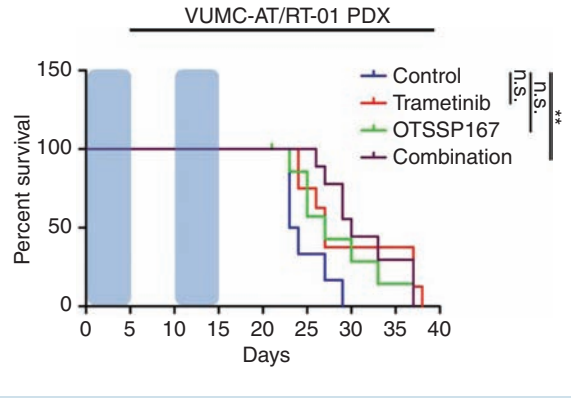

Fig. 6 Efficacy of OTSSP167 and trametinib in VUMC-AT/RT-01 xenograft-bearing mice. Kaplan–Meier curves showing survival of mice carrying VUMC-AT/RT-01 xenografts, treated twice for 5 consecutive days (blue area), separated by a 5-day recovery period, with OTSSP167 and/or trametinib. $^{**}P < 0.01$ (log-rank test).

Discussion

In the present study, we identify the embryonic kinase MELK, which is strongly upregulated in AT/RT cells compared with normal cerebral and cerebellar tissue, as a novel therapeutic target in atypical teratoid/rhabdoid tumors. Correspondingly, we show that inhibition of MELK by RNA interference or use of the small-molecule OTSSP167 (at low nanomolar concentrations) results in a strong antitumor effect in patient-derived neurosphere cultures. Given the efficacy of both pharmacological and shRNA-mediated MELK inhibition, the antitumor effect is unlikely to be unrelated to MELK, although some recent studies have shown efficacy of OTSSP167 in MELK^{null} tumor models, suggesting that off-target effects of the drug may still contribute to its antitumor efficacy in our study.[29,30] Combined inhibition of MELK and components of the MAPK signaling pathway, which has previously been shown to be activated in AT/RT,[9,10] synergistically decreases AT/RT cell viability. Previous research on the function of MELK in melanoma cells, and on recombinant MELK protein, has revealed MELK as a downstream effector of the MAPK signaling pathway, either via direct phosphorylation of MELK by MAPKs or via increased transcription of MELK by activation of the transcription factor E2F1.[12,14] In line with this, we observed a decrease in MELK protein levels in VUMC-AT/RT-01R and CHLA-AT/RT-02 cells treated with trametinib, although MELK levels of VUMC-AT/RT-01 cells were unaffected by MEK inhibition, and MELK expression slightly increased in CHLA-AT/RT-06 cells treated with trametinib, implying different molecular mechanisms of action between AT/RT models. As our RNA sequencing data showed no decrease in MELK RNA expression upon treatment of AT/RT cells with trametinib, this interaction most likely takes place on a posttranslational level. Intriguingly, inhibition of MELK by OTSSP167 reduced both the phosphorylation and expression of ERK1/2 in VUMC-AT/RT-01R and CHLA-AT/RT-02 cells, suggesting a reciprocal feedback loop between MELK and MAPK signaling in these cells, which may differ between subgroups of AT/RT, via as yet unknown mechanisms. In this case, MELK inhibition by OTSSP167 reduced RNA levels of MAP2K2 (ERK2) in AT/RT cells, implying an indirect transcriptional modulation of MAP2K2 by MELK. Further research is required to explain the molecular mechanisms underlying these observations. From a translational perspective, the high sensitivity of VUMC-AT/RT-01R cells to trametinib and the combination of OTSSP167 and trametinib, compared with VUMC-AT/RT-01 cells, suggest a differential sensitivity of AT/RT cells to MEK and MELK inhibition at diagnosis and relapse, which may have therapeutic implications, although our sample size was too small to draw definitive conclusions, owing to the lack of paired diagnosis-relapse models of AT/RT. Treatment of CNS malignancies is strongly impeded by the presence of the BBB, preventing chemotherapeutic drugs from reaching the tumor cells. Nonetheless, AT/RT often display strong contrast enhancement on MRI, and intensive chemotherapeutic regimens have shown to contribute to an improved survival of AT/RT patients, suggesting a functional deficit of the BBB in AT/RT.[2,3] We here identify several abnormalities of the vasculature of AT/RT in tumor tissue and VUMC-AT/RT-01, as well as CHLA-AT/RT-06 xenografts. Tumor tissue contained significantly fewer blood vessels compared with normal brain tissue, although these vessels were larger in diameter. Moreover, expression of GLUT1, a transporter expressed by BBB endothelial cells and a marker for BBB integrity, was strongly reduced in intratumoral blood vessels in both xenograft models, whereas expression of the BBB tight junction protein CLDN5 was maintained in VUMC-AT/RT-01 xenografts. Staining for CLDN5 in these tumors, however, did reveal a disorganization of tight junctions between endothelial cells of intratumoral blood vessels. These abnormalities were also observed in the original tumor tissue, the only exception being the presence of endothelial cells lacking CLDN5 expression in areas of microvascular proliferation in these samples. Taken together, these vascular abnormalities bear a striking resemblance to those observed in WNT subgroup medulloblastomas, which have been shown to possess a functionally defective BBB that allows chemotherapeutic agents to cross.[28] Importantly, both drugs investigated in the current study, OTSSP167 and trametinib, have been shown to poorly cross an intact BBB.[11,26] Nonetheless, treatment of AT/RT xenograft-bearing mice with this combination of drugs did result in a significant increase in median survival, thereby demonstrating the therapeutic implications of the observed BBB deficiencies in AT/RT and validating MEK and MELK as therapeutic targets for these tumors. Further research is required to determine if this is true for all AT/RT or limited to a certain subtype as in the case of medulloblastoma. Although our research is limited by the availability of representative AT/RT models and our understanding of the mechanisms behind the synergy between MEK and MELK inhibition, we present several important insights for (pre)clinical therapy development for these devastating tumors. Firstly, the apparent functional BBB deficits may explain the apparent clinical efficacy of non-BBB penetrable agents in the treatment of AT/RT, such as doxorubicin and etoposide. Moreover, it allows us to reconsider chemotherapeutic and targeted drugs for the

treatment of AT/RT, which were previously discarded for their lack of BBB penetration. Concurrently, the extent of and mechanisms behind the BBB disruption in AT/RT, as well as the representativity of the data we present in the current study for all subtypes of this tumor, need to be validated in future research to establish the definitive implications of our findings. Secondly, the proposed combination treatment of AT/RT with MEK and MELK inhibition may further be optimized to yield greater efficacy—for example, by investigating different treatment schedules or by choosing agents with more favorable pharmacokinetic properties. Additionally, we are likely underestimating the potential in our study, as the more sensitive VUMC-AT/RT-01R cells did not establish xenografts and could therefore not be treated in vivo. Moreover, this treatment strategy may be extrapolated to other rhabdoid tumors driven by loss of SMARCB1, such as malignant rhabdoid tumors of the kidney. Altogether, our study reveals functional, therapeutically exploitable BBB deficiencies in AT/RT, and establishes MELK as a novel therapeutic target for their treatment, mainly in combination with MEK inhibition.

Supplementary Material

Supplementary data are available at *Neuro-Oncology* online.

Keywords

atypical teratoid/rhabdoid tumor | blood-brain barrier | maternal embryonic leucine zipper kinase | preclinical therapy development | tumor models

Funding

This work was supported by the Egbers Foundation.

Conflict of interest statement. None of the authors declare any conflicts of interest.

Authorship statement. M.H.M. and E.H. conceived and designed the project. M.H.M., P.W., T.L., M.D.W, N.S., E.A., and M.Bu. developed and validated the in vitro and in vivo models used in the study. M.H.M., M.G.N., D.S.M., and P.W. performed the functional in vitro and western blotting experiments. M.B. and M.Bu. performed the immunohistochemistry experiments. T.N.P. performed the immunofluorescence experiments and vascular phenotyping of the AT/RT xenografts. J.K. provided bioinformatical expertise and support. M.C.G., L.E.W., M.Bu., and O.T. provided material and logistical support and advised on the project. G.J.K. and E.H. acquired funding and supervised the study. All authors contributed to writing the manuscript.

References

1. Chi SN, Zimmerman MA, Yao X, et al. Intensive multimodality treatment for children with newly diagnosed CNS atypical teratoid rhabdoid tumor. *J Clin Oncol.* 2009;27(3):385–389.
2. Ginn KF, Gajjar A. Atypical teratoid rhabdoid tumor: current therapy and future directions. *Front Oncol.* 2012;2:114.
3. Slavc I, Chocholous M, Leiss U, et al. Atypical teratoid rhabdoid tumor: improved long-term survival with an intensive multimodal therapy and delayed radiotherapy. The Medical University of Vienna experience 1992–2012. *Cancer Med.* 2014;3(1):91–100.
4. Kim KH, Roberts CW. Mechanisms by which SMARCB1 loss drives rhabdoid tumor growth. *Cancer Genet.* 2014;207(9):365–372.
5. Roberts CW, Biegel JA. The role of SMARCB1/INI1 in development of rhabdoid tumor. *Cancer Biol Ther.* 2009;8(5):412–416.
6. Johann PD, Erkek S, Zapatka M, et al. Atypical teratoid/rhabdoid tumors are comprised of three epigenetic subgroups with distinct enhancer landscapes. *Cancer Cell.* 2016;29(3):379–393.
7. Torchia J, Golbourn B, Feng S, et al. Integrated (epi)-genomic analyses identify subgroup-specific therapeutic targets in CNS rhabdoid tumors. *Cancer Cell.* 2016;30(6):891–908.
8. Viswanathan SR, Powers JT, Einhorn W, et al. Lin28 promotes transformation and is associated with advanced human malignancies. *Nat Genet.* 2009;41(7):843–848.
9. Weingart MF, Roth JJ, Hutt-Cabezas M, et al. Disrupting LIN28 in atypical teratoid rhabdoid tumors reveals the importance of the mitogen activated protein kinase pathway as a therapeutic target. *Oncotarget.* 2015;6(5):3165–3177.
10. Rubens JA, Wang SZ, Price A, et al. The TORC1/2 inhibitor TAK228 sensitizes atypical teratoid rhabdoid tumors to cisplatin-induced cytotoxicity. *Neuro Oncol.* 2017;19(10):1361–1371.
11. Meel MH, de Gooijer MC, Guillén Navarro M, et al. MELK inhibition in diffuse intrinsic pontine glioma. *Clin Cancer Res.* 2018;24(22):5645–5657.
12. Badouel C, Körner R, Frank-Vaillant M, Couturier A, Nigg EA, Tassan JP. M-phase MELK activity is regulated by MPF and MAPK. *Cell Cycle.* 2006;5(8):883–889.
13. Ganguly R, Hong CS, Smith LG, Kornblum HI, Nakano I. Maternal embryonic leucine zipper kinase: key kinase for stem cell phenotype in glioma and other cancers. *Mol Cancer Ther.* 2014;13(6):1393–1398.
14. Janostiak R, Rauniyar N, Lam TT, et al. MELK promotes melanoma growth by stimulating the NF-κB pathway. *Cell Rep.* 2017;21(10):2829–2841.
15. Ji W, Arnst C, Tipton AR, et al. OTSSP167 abrogates mitotic checkpoint through inhibiting multiple mitotic kinases. *PLoS One.* 2016;11(4):e0153518.
16. Jiang P, Zhang D. Maternal embryonic leucine zipper kinase (MELK): a novel regulator in cell cycle control, embryonic development, and cancer. *Int J Mol Sci.* 2013;14(11):21551–21560.
17. Chung S, Suzuki H, Miyamoto T, et al. Development of an orally-administrative MELK-targeting inhibitor that suppresses the growth of various types of human cancer. *Oncotarget.* 2012;3(12):1629–1640.
18. Joshi K, Banasavadi-Siddegowda Y, Mo X, et al. MELK-dependent FOXM1 phosphorylation is essential for proliferation of glioma stem cells. *Stem Cells.* 2013;31(6):1051–1063.
19. Minata M, Gu C, Joshi K, et al. Multi-kinase inhibitor C1 triggers mitotic catastrophe of glioma stem cells mainly through MELK kinase inhibition. *PLoS One.* 2014;9(4):e92546.
20. Nakano I, Joshi K, Visnyei K, et al. Siomycin A targets brain tumor stem cells partially through a MELK-mediated pathway. *Neuro Oncol.* 2011;13(6):622–634.

21. Meel MH, Sewing ACP, Waranecki P, et al. Culture methods of diffuse intrinsic pontine glioma cells determine response to targeted therapies. *Exp Cell Res.* 2017;360(2):397–403.
22. Meel MH, Metselaar DS, Waranecki P, Kaspers GJL, Hulleman E. An efficient method for the transduction of primary pediatric glioma neurospheres. *MethodsX.* 2018;5:173–183.
23. Birks DK, Donson AM, Patel PR, et al. High expression of BMP pathway genes distinguishes a subset of atypical teratoid/rhabdoid tumors associated with shorter survival. *Neuro Oncol.* 2011;13(12):1296–1307.
24. Peferoen LA, Breur M, van de Berg S, et al. Ageing and recurrent episodes of neuroinflammation promote progressive experimental autoimmune encephalomyelitis in Biozzi ABH mice. *Immunology.* 2016;149(2):146–156.
25. Ianevski A, He L, Aittokallio T, Tang J. SynergyFinder: a web application for analyzing drug combination dose-response matrix data. *Bioinformatics.* 2017;33(15):2413–2415.
26. de Gooijer MC, Zhang P, Weijer R, Buil LCM, Beijnen JH, van Tellingen O. The impact of P-glycoprotein and breast cancer resistance protein on the brain pharmacokinetics and pharmacodynamics of a panel of MEK inhibitors. *Int J Cancer.* 2018;142(2):381–391.
27. Vaidhyanathan S, Mittapalli RK, Sarkaria JN, Elmquist WF. Factors influencing the CNS distribution of a novel MEK-1/2 inhibitor: implications for combination therapy for melanoma brain metastases. *Drug Metab Dispos.* 2014;42(8):1292–1300.
28. Phoenix TN, Patmore DM, Boop S, et al. Medulloblastoma genotype dictates blood brain barrier phenotype. *Cancer Cell.* 2016;29(4):508–522.
29. Giuliano CJ, Lin A, Smith JC, Palladino AC, Sheltzer JM. MELK expression correlates with tumor mitotic activity but is not required for cancer growth. *eLife.* 2018;7.
30. Lin A, Giuliano CJ, Sayles NM, Sheltzer JM. CRISPR/Cas9 mutagenesis invalidates a putative cancer dependency targeted in on-going clinical trials. *eLife.* 2017;6.